Geophysical Research Letters

RESEARCH LETTER
10.1029/2019GL083749

Internal Structure of a Seafloor Massive Sulfide Deposit by Electrical Resistivity Tomography, Okinawa Trough

K. Ishizu[1], T. Goto[1,2], Y. Ohta[1], T. Kasaya[3], H. Iwamoto[3,4], C. Vachiratienchai[5], W. Siripunvaraporn[6,7], T. Tsuji[8], H. Kumagai[3], and K. Koike[1]

[1]Department of Urban Management, Kyoto University, Kyoto, Japan, [2]Now at Graduate School of Life Science, University of Hyogo, Hyogo, Japan, [3]Japan Agency for Marine-Earth Science and Technology (JAMSTEC), Kanagawa, Japan, [4]Now at Nippon Marine Enterprises, Ltd., Kanagawa, Japan, [5]Curl-E Geophysics Co. Ltd., Thailand, [6]Department of Physics, Faculty of Science, Mahidol University, Bangkok, Thailand, [7]ThEP Center, Commission on Higher Education, Bangkok, Thailand, [8]Department of Earth Resources Engineering, Kyushu University, Fukuoka, Japan

Abstract Although seafloor massive sulfide (SMS) deposits are crucially important metal resources that contain high-grade metals such as copper, lead, and zinc, their internal structures and generation mechanisms remain unclear. This study obtained detailed near-seafloor images of electrical resistivity in a hydrothermal field off Okinawa, southwestern Japan, using deep-towed marine electrical resistivity tomography. The image clarified a semi-layered resistivity structure, interpreted as SMS deposits exposed on the seafloor, and another deep-seated SMS layer at about 40-m depth below the seafloor. The images reinforce our inference of a new mechanism of SMS evolution: Upwelling hydrothermal fluid is trapped under less-permeable cap rock. The deeper embedded SMS accumulates there. Then hydrothermal fluids expelled on the seafloor form exposed SMS deposits.

Plain Language Summary Hydrothermal circulation of seawater through the permeable ocean crust engenders formation of seafloor massive sulfide (SMS) deposits, which present high potential for metal mining. Geophysical surveys using modes such as electrical and electromagnetic methods have revealed that SMS deposits exhibit lower resistivity than the surrounding host rock. However, because detailed geophysical images of internal structures of SMS deposits are lacking, the spatial distribution of SMS deposits and the evolutionary processes of SMS deposits remain unclear. For this study, we applied a deep-towed marine electrical resistivity tomography (ERT) system to capture detailed images of electrical resistivity structures of SMS deposits in the Iheya North hydrothermal field, Okinawa Trough, southwestern Japan. An optimal sub-seafloor resistivity section reveals a semi-layered structure consisting of double low-resistivity SMS layers: exposed and deep-seated ones. Between the SMS layers, a cap rock layer is recognized as a moderately resistive zone. This detailed structure offers an explanation of how the SMS deposits accumulate: Hydrothermal fluids upwelling from the deep crust are trapped by less-permeable cap rock, which results in the precipitation and accumulation of SMS deposits below the cap rock. Then fluids passing through the cap rock to the seafloor produce SMS deposits on the seafloor.

Key Points:
- Deep-towed marine electrical resistivity tomography revealed massive sulfide deposits on the seafloor as low-resistivity zones
- Low-resistivity zones are semi-layered with deposits exposed on the seafloor and other deposits at 40-m depth below the seafloor
- Detailed near-seafloor images of electrical resistivity offer an explanation of how the SMS deposits accumulate

Supporting Information:
- Supporting Information S1

Correspondence to:
K. Ishizu,
ishizu.keiichi.77z@st.kyoto-u.ac.jp

Citation:
Ishizu, K., Goto, T., Ohta, Y., Kasaya, T., Iwamoto, H., Vachiratienchai, C., et al. (2019). Internal Structure of a Seafloor Massive Sulfide Deposit by Electrical Resistivity Tomography, Okinawa Trough. *Geophysical Research Letters*, *46*. https://doi.org/10.1029/2019GL083749

Received 23 MAY 2019
Accepted 12 SEP 2019
Accepted article online 16 SEP 2019

1. Introduction

Hydrothermal circulation below the seafloor is a process of heat and material exchange between seawater and the crust (Stein & Stein, 1992). Fluid convection caused by magmatic intrusion occurs at mid-ocean ridges, back-arc spreading centers, volcanic arcs, and so on (Boschen et al., 2013). Such seafloor hydrothermal systems often have accompanying seafloor massive sulfide (SMS) deposits, which offer high potential for mining of metals with high economic value (Hannington et al., 1995; Humphris et al., 1995; Rona et al., 1991). The major metal elements are copper, lead, zinc, gold, and silver (Bartetzko et al., 2006; Spagnoli et al., 2016). Their high metal concentrations can meet global demand for metal resources. Therefore, SMS deposits are attractive for next-generation mining (Lipton, 2012).

A map of the internal structures of a seafloor hydrothermal system provides a key to elucidating the SMS deposit generation mechanisms. In past studies, seafloor drilling surveys have been conducted for the lithological studies of SMS deposits. One of the best-studied hydrothermal areas is the Trans-Atlantic

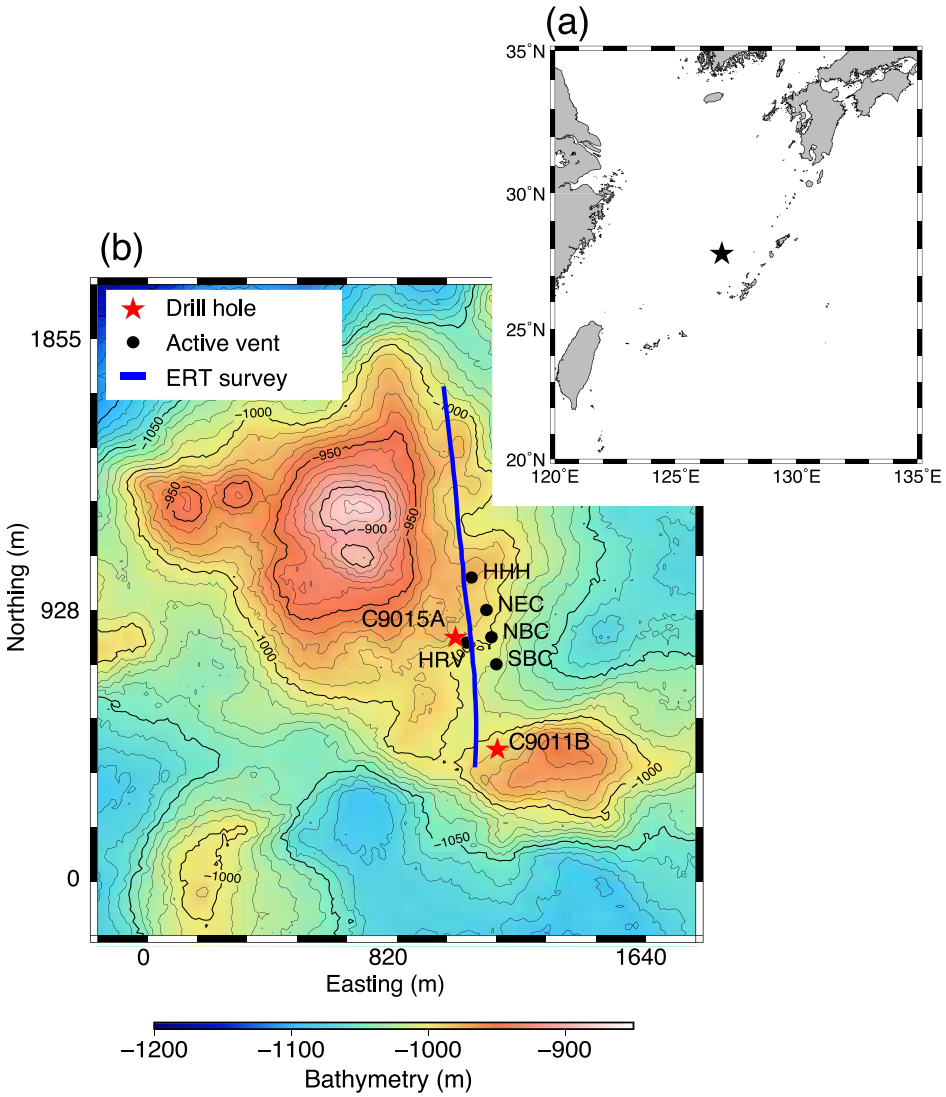

Figure 1. Maps of the study area. (a) Location of the Iheya North hydrothermal field, Okinawa Trough, southwestern Japan shown as a black star. (b) Event map of the Iheya North field. Red stars denote the Integrated Ocean Drilling Program drilling sites (C9015A and C9011B). Black circles denote hydrothermal fluid venting sites (SBC, HRV, NBC, NEC, and HHH). The blue line represents a survey profile with the towed electrical resistivity tomography (ERT) system.

Geotraverse (TAG) hydrothermal field in the mid–Atlantic Ocean (e.g., Humphris et al., 1995; Petersen et al., 2000). The Ocean Drilling Program revealed a lens-shaped ore body beneath the mound and an underlying upflow zone through the volcanic rocks that host the deposit (e.g., Humphris et al., 1995). Other hydrothermal fields such as in the Iheya North Knoll (Takai et al., 2011) and Palinuro Seamount (Petersen et al., 2014) were also investigated using boreholes. Tornos et al. (2015) compiled existing information of SMS deposits and proposed various models of SMS mineralization. However, the generation mechanisms of SMS remain unclear because of a lack of detailed internal images of SMS deposits. Although seafloor drilling is a powerful tool, its use is limited because it entails high costs. Even if numerous drillings are conducted, geophysical images have been requested to fill gaps among boreholes.

Various efforts to image and estimate SMS deposits have been undertaken using geophysical methods. Electrical and electromagnetic (EM) geophysical surveys are suitable for mapping the distribution of SMS deposits because the deposits show lower resistivity than the surrounding host rocks (Komori et al., 2017; Spagnoli et al., 2016). In the TAG mound, pilot EM surveys revealed sub-seafloor low-resistive areas, possibly related to SMS deposits (Cairns et al., 1996; Von Herzen et al., 1996). Haroon et al. (2018) and Gehrmann

et al. (2019) presented two-dimensional (2-D) inversion results across the TAG mounds using the towed controlled-source EM survey (Constable et al., 2016). They found low-resistive zones immediately beneath the seafloor with greater than 50-m thickness. These towed controlled-source EM surveys achieved both deeper penetration depth (~300 m) and dense spatial measurements. However, they had low sensitivity to near-seafloor structures because of the limited number of receivers and their survey configuration. Some new equipment has been designed for the near-seafloor resistivity mapping but with limited penetration depth of less than several meters (Kowalczyk, 2008). Other new surveys have deeper penetration to tens to hundreds of meters (Constable et al., 2018; Imamura et al., 2018; Müller et al., 2018; Safipour et al., 2017; Safipour et al., 2018). However, the measurements should be done as stationary (with the fixed source, receivers, or both) lacking dense spatial samplings. In fact, high-resolution images of resistivity structures below the seafloor in hydrothermal areas (e.g., to 50-m depth with spatial resolution of 10 m) have never been reported, even though such imaging is necessary to discuss the evolution mechanisms of SMS deposits attributable to high spatial heterogeneities that have been inferred from drilling studies.

We specifically examine a deep-towed marine electrical resistivity tomography (ERT) system with multiple electrodes to image such detailed electrical resistivity of SMS deposits. It has higher efficiencies of spatial coverage and resolution in the shallow sub-seafloor depth than other marine EM methods. This survey system was developed first for detecting shallowly existing gas hydrate (Goto et al., 2008; Chiang et al., 2012). The ERT system has often been used for near-surface exploration on land (also designated as direct current resistivity survey) with several stationary electrodes, but this marine ERT system tows multiple electrodes for increasing both the horizontal resolution near the seafloor and the total length of the survey profile.

Our target area is the Iheya North hydrothermal field, mid–Okinawa Trough, southwestern Japan (Figure 1). The Okinawa Trough, a back-arc basin of the Ryukyu arc-trench system, is presumed to be in the initial stage of continental rifting, although some controversy persists about the commencement of Okinawa Trough rifting (Letouzey & Kimura, 1986). A hydrothermal area discovered on the Iheya North Knoll in 1995 (Momma et al., 1996) has since been investigated intensively (Kasaya et al., 2015; Kumagai et al., 2010; Masaki et al., 2011; Miyoshi et al., 2015; Nakagawa et al., 2005; Takai et al., 2006; Tsuji et al., 2012). The Integrated Ocean Drilling Program (IODP) Expedition 331 was also conducted in the area by the deep-sea drilling vessel Chikyu. Core samples of IODP Expedition 331 strongly resemble the black ores in kuroko deposits of the Miocene age in Japan (Expedition 331 Scientists, 2010). More recently, additional drilling was implemented at the CK14-04 and CK16-01 cruises (Expeditions 907, 908) by drilling vessel Chikyu. The accumulated survey data indicate this area as suitable for our detailed imaging of SMS deposits.

2. Method of Marine Electrical Resistivity Tomography

To date, ERT has been used for land areas and for shallow water areas (e.g., Allen & Merrick, 2007; Inoue, 2005; Lile et al., 1994) and even for deep water areas (Goto et al., 2008). For ERT survey, an electrical current is passed through two electrodes. The resultant voltages are then measured through other paired electrodes. The towed long tail in this system consists of cables with lengths of about 180 m (Figure 2a). The system closely follows the earlier version developed by Goto et al. (2008) with slight modification of the electrode configuration (Goto et al., 2013; Kasaya et al., 2018). The waveform of the transmitted current is a square wave with a period of 15 s. The maximum output current is 15 A. The deep-tow system has a conductivity-temperature depth sensor and an altimeter relative to the seafloor. The apparent resistivity values of the dipole-dipole array are estimated using least-squares method at every 15 s, with segments corresponding horizontally to a sampling rate of 7.5 m. Other detailed descriptions of the system are shown in Figure 2a and Supporting Information, Text S1. The system affords high horizontal resolution by continuous towing of multiple electrodes, in addition to the simplicity of data acquisition and analysis. The SMS deposits are generally located at water depths greater than 900 m. The topography in hydrothermal regions is quite complex. Simple systems such as the deep-towed marine ERT with real-time acoustic navigation system and carefully planned towing routes based on the detailed bathymetric map are well suited to SMS exploration under such environments.

The Iheya North hydrothermal field of the Okinawa Trough is about 150 km NNW distant from Okinawa Island (Figure 1a). The ERT data were collected during the YK 14–19 cruise survey (R/V Yokosuka, JAMSTEC) at the active hydrothermal region, where hydrothermal fluid venting sites have been observed (Figure 1b). The system

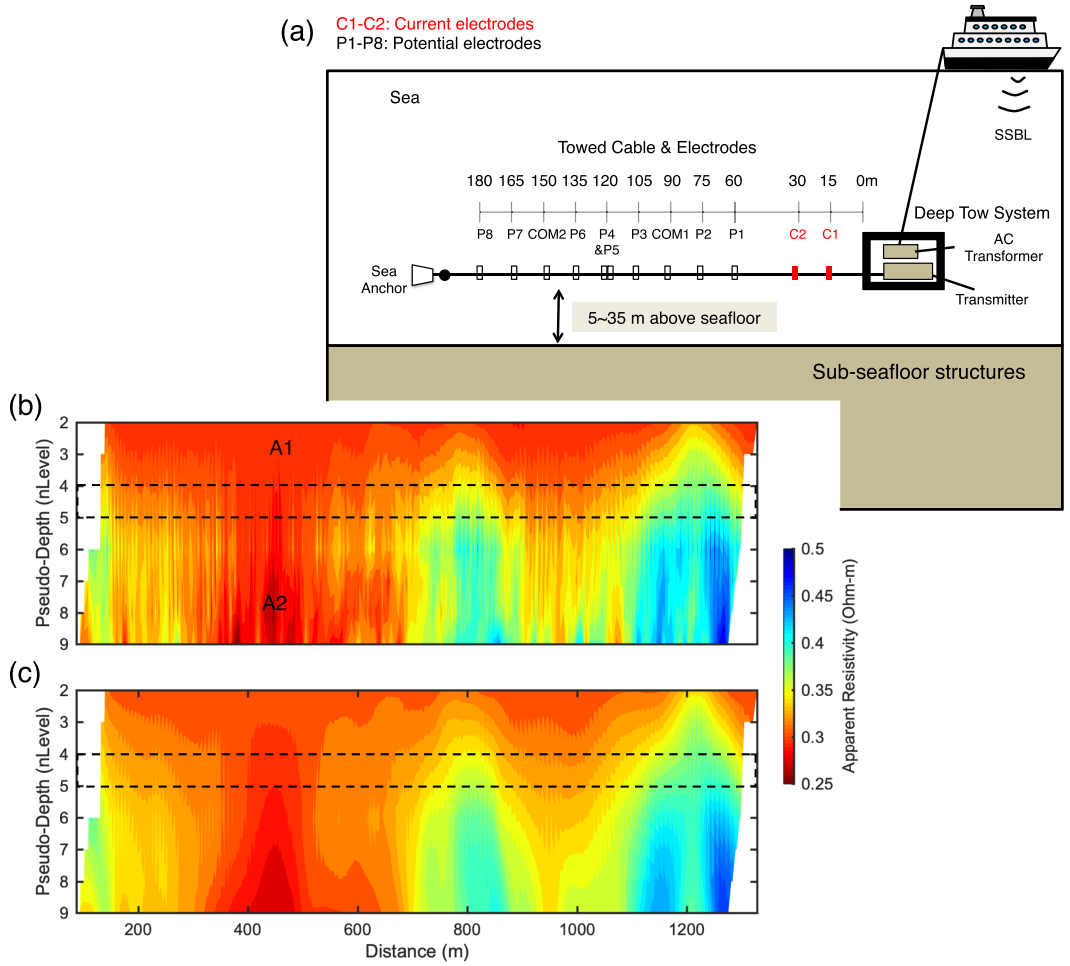

Figure 2. (a) Schematic diagram of the deep-towed marine electrical resistivity tomography system. Two current electrodes C1 and C2 and eight potential electrodes P1–P8 are attached to the cable together with two reference electrodes COM1 and COM2. The voltage difference is measured using each 15-m dipole: P1–P2, P2–COM1, COM1–P3, P3–P4, P5–P6, P6–COM2, COM2–P7, and P7–P8. Acoustic transponders were attached respectively to the deep tow system and end of cable (a solid circle). (b) Pseudo-section of the observed data. Pseudo-depth shows the n level of Tx-Rx distance ($15 \times n$). A1 and A2 show the low apparent resistivity areas. (c) Pseudo-section of the response from the inverted model (Figure 3a). Missing observed data points at n levels (4 and 5) enclosed by dashed lines were interpolated from neighboring points. AC = alternating current; SSBL = super-short baseline.

was towed from the south to north with altitude of 5–50 m above the seafloor. The electrode pairs of COM1–P3 and P3–P4 (n levels 4 and 5) were, unfortunately, unavailable because of system troubles. The number of collected data as apparent resistivity was 966. The averaged error values of the observed apparent resistivity are, respectively, 0.14%, 0.22%, 1.70%, 2.04%, 2.39%, and 3.23% for n levels 2, 3, 6, 7, 8, and 9.

We converted the observed ERT responses into a 2-D resistivity model by our own nonlinear regularized inversion method (Ishizu et al., 2017; Ishizu et al., 2019). The 2-D ERT forward modeling problem (e.g., Coggon, 1971; Dey & Morrison, 1979; Xu et al., 2000) was solved using finite element method with unconstructed meshes generated by Triangle (Shewchuk, 1996), which is used in various EM surveys because of high flexibility to complex structures (e.g., Key & Weiss, 2006). Unconstructed meshes are suitable for modeling the complex topography of hydrothermal fields. We applied Occam's algorithm proposed by Constable et al. (1987) to this inverse problem. Occam's inversion seeks the smoothest sub-seafloor model that has an appropriate misfit level between observed and calculated apparent resistivity values (e.g., Key, 2009; Siripunvaraporn & Egbert, 2000; Vachiratienchai & Siripunvaraporn, 2013). More details of our forward modeling and inversion algorithm are summarized in Texts S2 and S3. The initial and prior models for the inversion are 1.0 Ω·m homogeneous half-space below the seafloor. The grid number for the forward

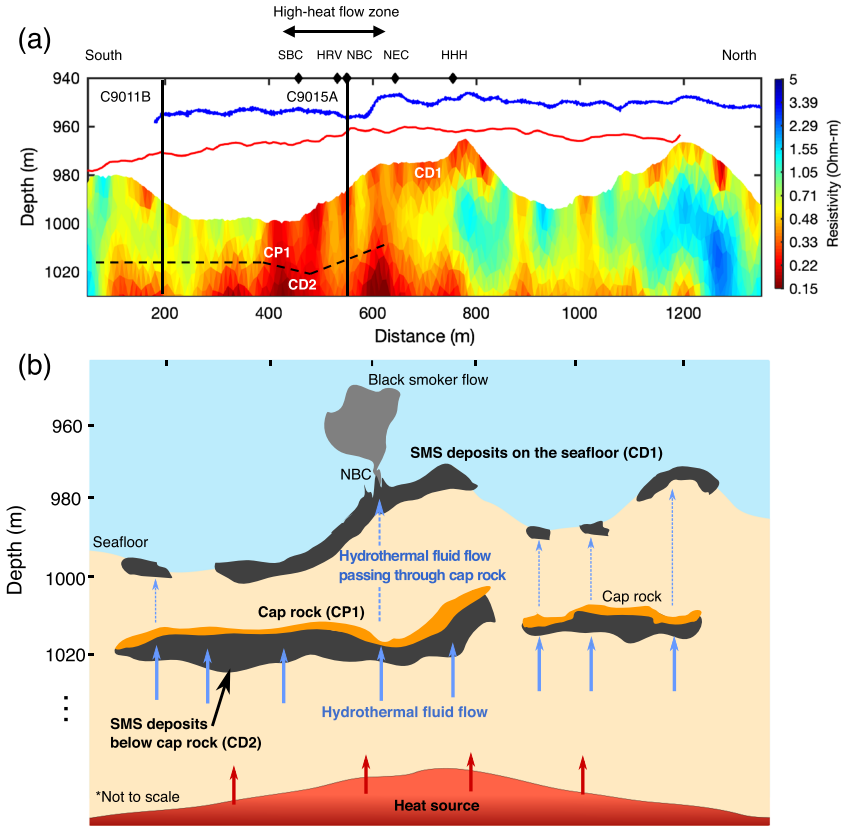

Figure 3. (a) Inverted resistivity model from the electrical resistivity tomography survey data. Blue and red lines respectively show the head and the tail positions of the deep-towed system. Black lines are locations of seafloor drilling. Black diamonds show the horizontal position of observed hydrothermal vents, presented in Figure 1b. The black dashed line is a strong seismic reflector obtained during cruises KR 10-02 (Tsuji et al., 2012). CD1 and CD2 denote conductive zones, which imply seafloor massive sulfide (SMS) deposits. CP1 is a cap rock zone. The black double arrow indicates a high-heat flow zone (Masaki et al., 2011). (b) Schematic model of evolution of SMS deposits inferred from our inverted model; it is not to scale.

modeling was 16,327; the number of unknown parameters was 6,186 without updating the seawater resistivity. The error floor was set as 2% of the observed apparent resistivity. The average and standard deviation of the sea resistivity measured using conductivity-temperature depth during the towing were, respectively, 0.3062 and 0.373×10^{-3} Ω·m. The seawater resistivity was fixed in the modeling as this average.

3. Results and Discussion

The apparent resistivity obtained using our marine ERT system indicates electrically conductive features below the seafloor. The pseudo-section of observed apparent resistivity is presented in Figure 2b. At short separations between current and potential electrodes (with n level of 2–3), low apparent resistivity values are observed at horizontal locations of 200–700 m (A1 in Figure 2b). The values are about 0.3 Ω·m, which is lower than the seawater resistivity, implying the existence of the conductive zones below the seafloor. Moreover, at horizontal locations of 350–500 m, the lowest apparent resistivity (A2 in Figure 2b) is discovered under the longer separations (e.g., n level of 7–9). The observed error of apparent resistivity is about 0.14–0.22% at an n level of 2–3 and 2.39–3.23% at an n level of 8–9, so that the low apparent resistivity values at A1 and A2 are valid. They possibly correspond to extremely conductive zones buried deep below the seafloor.

Cable slack and pitching errors can distort the observed data. However, these effects are negligible compared to responses from the structures (Text S4 and Figures S4 and 5). The effect by yaw of towed cable is complicated because the lined electrode array was not perpendicular to the assumed strike of the 2-D structure (Figure S6). Although no published papers present discussion of this effect in 2-D inversion

numerically, field examples frequently found proper subsurface structures in such cases (e.g., Kwon et al., 2005). We believe that our ERT can also image the sub-seafloor 2-D structure properly, although it might be distorted slightly because of yawing.

The inversion result (Figure 3a) is consistent with the features inferred from the observed pseudo-section of apparent resistivity. The initial root-mean-square misfit between observed and calculated apparent resistivity values was 6.5. Subsequently, it reached 2.2 after the third iteration through the inversion process. The apparent resistivity pseudo-section calculated from this model (Figure 2c) closely matches with the observed data, especially including good fits to the low apparent resistivity values (A1 and A2 in Figure 2b). Based on synthetic inversion tests with sub-seafloor models having a simple low-resistivity anomaly (Ishizu et al., 2019), the approximate maximum sounding depth of 45 m below the towed cable can be well resolved. In this survey, the area shallower than 1,012 m from the sea surface (i.e., the averaged towed depth, 967 m, plus 45 m) can be well resolved. Although the area deeper than 1,012 m has lower resolution than the shallower part, it still has sensitivity and necessity for explaining the observed ERT data (Text S5). Based on these sensitivity tests, we chose 0.032 of the normalized sensitivity (maximum value is 1.0; shown in Figure S8) as a threshold of the resolved areas, corresponding to about 1,030-m depth below the sea surface.

Proof of the reliability of the inverted resistivity was found from borehole C9011B and C9015A data obtained during the CK14-04 cruise (Figure 1b). The averaged resistivity values to the depth of about 30 m below seafloor (mbsf) obtained through logging while drilling (LWD) were, respectively, about 0.3 Ω·m along C9015A and about 0.8 Ω·m along C9011B (Takai et al., 2015). These averaged values are agreeable with the inversion result in which C9015A is located in the more conductive seafloor than C9011B. Small-scale vertical spatial variations of LWD resistivity along each borehole were not recovered in the inverted model because of the limited resolution of the ERT data with the smoothness constraint in the inversion scheme (Figure S7). The inverted model has strong lateral variations near the seafloor. To investigate the ERT inversion ability of resolving small structures (25 × 10 m) near the seafloor, we conducted a sensitivity test using synthetic data. The inversion well recovered the small structures (Figure S13) because of the high horizontal sensitivity.

The inversion result reveals sub-seafloor electric conductive zones of around 0.2 Ω·m or less. The resistivity section also shows semi-layered structures (Figure 3): the shallow conductive zone (CD1) and the deeply buried one (CD2). We applied sensitivity tests by forward modeling (e.g., Schwalenberg et al., 2002) to evaluate the existence of conductivity anomalies CD1 and CD2, the resistivities of which are replaced respectively with the background resistivity of 1.0 Ω·m. Results for which CD1 and CD2 were replaced show that the root-mean-square misfit increased from 2.2 to 5.0 and 3.4, respectively (Figures S11 and S12). Sensitivity studies using the inversion algorithm show that these semi-layered conductive zones, CD1 and CD2, are necessary to explain the observed low apparent resistivity (A1 and A2), as described in Text S5. The extremely low-resistivity value compared to the background one (1.0 Ω·m) is consistent with resistivity values of SMS deposits measured in the hydrothermally active area (Cairns et al., 1996; von Herzen et al., 1996). On the seafloor above CD1 and CD2, several hydrothermal fluid venting sites are observed (Kawagucci et al., 2013) together with high heat flow anomalies (Masaki et al., 2011). Therefore, CD1 and CD2 might be attributable to conductive SMS deposits or a conductive hydrothermal fluid reservoir below the seafloor.

The occurrences of SMS deposits are linked to local three-dimensional (3-D) topography at horizontal distance of 750 m along our profile, thus possible distortions of the 3-D topographic effects must be considered. An estimated model by 2-D inversion of data from a 3-D conductive structure might contain artifacts below and next to the conductive mound (CD1). However, we believe that the conductive mound can be resolved as discussed in the numerical studies by Haroon et al. (2018). Higher resistivities were recovered around horizontal distance of 1,200 m, where there is a strong topography adjacent to the profile (Figure 3a). However, the adjacent volcanic summit is located far from our towed profile (300 m). There is no large relief around the profile at horizontal distance of 1,200 m (Figure 1a). Therefore, the topographic effects are negligible compared to responses from the resistivity structures below the profile.

The rock resistivity depends on diverse factors such as porosity, temperature, and salinity of pore fluids and on the amounts of metallic minerals (e.g., Archie, 1942; Chave et al., 1991; Dakhnov, 1962; Quist & Marshall, 1968; Revil et al., 2015a, 2015b). For quantitative discussion of the causes of high conductivity in CD1 and CD2, we specifically examine a rock-physics modeling of SMS deposits reported by Ohta et al. (2018) based on laboratory measurements of rock samples from hydrothermal active areas in the Okinawa Trough (Text

S6). The porosity values of 0–10 and 20–30 mbsf are also assumed to be less than 25% and 10%, respectively, based on the drilled samples in the IODP Expedition 331 (Hole C0016; Takai et al., 2011).

For explanation of the deeply buried conductive zone (CD2, less than 0.2 Ω·m), with porosity less than 10% and temperature of 300 °C based on the measured maximum value of hydrothermal fluid at NBC by Kawagucci et al. (2011), the rock-physics equation gives the conductive SMS minerals with volume amount greater than 9% (Figure S15). In other words, under the assumed porosity (≤10%), high temperatures (high conductivity) of pore fluids alone cannot explain the low resistivity of less than 0.2 Ω·m in CD2. The existence of conductive SMS minerals is consistent with rock-core observations at 27–45 mbsf of Hole C0016, drilled at NBC, containing approximately 5% sulfide with very fine-grained pyrite (Takai et al., 2011). Similar contents of fine-grained sulfide minerals (3%: Takai et al., 2015) were also confirmed in the recovered cores at about 23–31 mbsf at Hole C9015B drilled by the CK14-04 cruise. For the shallow seafloor conductive zone (CD1, around 0.2 Ω·m), the same equation indicates absence of conductive SMS minerals under porosity of 25% and temperature of 300 °C (Figure S15). However, X-ray diffraction analysis of rock samples from the Iheya North hydrothermal field indicated the volume amount of conductive SMS minerals as 18–49% (Ohta et al., 2018). The temperature is expected to be much lower than 300 °C because of cooling by seawater. Therefore, CD1 also requires greater amounts of conductive SMS (e.g., greater than 9% at a temperature of about 100 °C). Note that we only discussed conductive SMS. The cores from Hole C0016B at 6–9 mbsf consist of massive sulfide ore containing 40–60% sphalerite (nonconductive SMS), 10–20% pyrite, and a few percent each of galena and chalcopyrite (Takai et al., 2011). The total amount including both conductive and nonconductive SMS would be much more than that of only conductive SMS.

The seawater salinity also decreases the resistivity with a linear relation (Keller, 1988). The minimum salinity measured at discharge zones above vents is 30% smaller than that of seawater (Kawagucci et al., 2011). However, such slight fluctuation of seawater salinity cannot explain the low resistivity of 0.2 Ω·m. We also devote attention to the clay minerals. Actually, core samples obtained at depth 30 mbsf (C0016) contain chlorite (Miyoshi et al., 2015). However, laboratory measurements by Ohta et al. (2018) demonstrate a minor effect of clay in electrical conduction. In addition, logging data measured in land hydrothermal areas often show low resistivity at the clay-rich layer, but the typical value is around 1.0 Ω·m (e.g., at drilling around Mt. Aso, Japan, as reported by New Energy and Industrial Technology Development Organization, 1995). This resistivity value is insufficient for causing low resistivity (0.2 Ω·m). Therefore, we conclude that conductive zones CD1 and CD2 can both be attributed to SMS deposits.

The semi-layered resistivity structure is supported by the multichannel seismic reflection data recorded on the KR 10-02 cruise (Tsuji et al., 2012). To characterize the shallow structures close to the seafloor precisely, we carefully analyzed the shallow reflectors in seismic data analysis (e.g., velocity analysis). The seismic profile highlights strong reflectors with positive polarity below the venting sites (southern half of our survey profile; Figure 3a), which implies the existence of rock layers with high-acoustic impedance. The reflective layer, which is recognized horizontally and as extending widely below the seafloor, corresponds to the top of the deep conductive zone, CD2. This observation supports no indication of a huge reservoir of hydrothermal fluids at CD2. Altered volcanic rocks with quartz-chlorite-pyrite and pyrite-anhydrite veins were found in cores recovered from Hole C0016 (27–45 mbsf; Takai et al., 2011). Another drilling result at 23–31 mbsf in Hole C9015B indicated highly silicified quartz-rich rocks with 3% fine-grained SMS (Takai et al., 2015). The altered volcanic and silicified quartz-rich rocks are probably harder than the near-seafloor unconsolidated materials, resulting in strong amplitude layers with positive polarity. In addition, the layers might have lower permeability than their surroundings because gypsification of the anhydrite and silicification engender rapid closure of pore spaces and fractures in the host rock.

From the interpretations presented above, a possible mechanism of formation of the semi-layered SMS deposits can be inferred as the following (Figure 3b). Because of the good correspondence of the conductive zones (CD1 and CD2) with the hydrothermal vents and high heat flows, hydrothermal fluids are expected to ascend from the deep parts of CD1 and CD2. The hydrothermal waters can be captured by less-permeable cap rocks (CP1 in Figure 3), as inferred from the seismic reflectors and drillings. The trapped hydrothermal fluids precipitated SMS minerals below CP1, thereby forming conductive SMS deposits in CD2. The hydrothermal fluids passing through the cracks or fractures remaining in the cap rocks (CP1) can develop SMS deposits at CD1 by mixture with seawater. This scenario is verified by the moderately low-resistivity connections between the exposed (CD1) and deeply buried conductive zones (CD2) in the resistivity structure, as seen

at horizontal locations 100–200, 400–800, 900, 1,000, and 1,200 m (Figure 3a). These connections imply the pathways of hydrothermal fluids.

Similar two-layer or multilayered SMS structures have been found from drilling in the Iheya North hydrothermal field, not along our profile. The LWD exhibited two sequences of large variation in gamma ray and resistivity, each of which indicated a high natural gamma-ray radiation zone, a low-resistivity zone (<0.3 Ω·m), and a low-radiation/high-resistive zone from shallow to deep depths (Takai et al., 2015). This sequence can be interpreted as a K-rich alteration zone, a buried sulfide zone, and low-K hard (silicified) sediments (Saito et al., 2015). Although the two-layer SMS deposits in the Okinawa Trough were revealed by the seafloor drilling, the number of these boreholes was limited. The recovery rate of the core is generally low in the hydrothermal field. Therefore, our resistivity structure is the first detailed image of the two-layer SMS deposits in the Okinawa Trough and also the first ever reported in the world. Such complex (two-layered or multilayered) SMS deposits under two or more styles of mineralization are necessary in most cases (in the review by Tornos et al., 2015) and might be rather normal. In the review, the near-seafloor and deeply buried SMS deposits found in this study were classified into two types: SMS in seafloor mounds and black smoker chimneys in oxic environments and SMS under sub-seafloor mineral replacement. Detailed mechanisms of simultaneous or sequential growth of SMS deposits with two layers or multilayers (e.g., fluid migration and mineralization processes in the layers CD1 and CD2) will be discussed in the near future based on our resistivity structure and the rock-core samples obtained by drilling in this area.

4. Conclusions

We applied a deep-towed ERT system to clarify the electrical resistivity structures of SMS deposits in the Iheya North hydrothermal field, the Okinawa Trough, southwestern Japan. The resistivity image by the inversion analysis revealed that the highly conductive zones below the seafloor were consistent with observed hydrothermal venting sites and heat anomalies. This high conductivity is probably attributable to rich conductive SMS minerals, not only to high-temperature fluids, clay minerals, and salinity of pore fluids. Our resistivity cross section indicates a semi-layered structure consisting of exposed and deeply embedded SMS deposits. The cap rock layer is also inferred from a seismic reflection survey and seafloor drillings. Integration of all results suggests a possible generation mechanism of SMS deposits. Hydrothermal fluids migrate from deep parts to the seafloor. They are captured by the cap rocks, where lower SMS deposits are generated below the seafloor. Fluids passing through fractures in the cap rocks to the seafloor develop the upper SMS deposits on the seafloor. Our study represents the first reported success in detailed imaging of SMS deposits, which demonstrates the effectiveness of the marine deep-towed ERT system for exploration and characterization of SMS deposits.

Acknowledgments
The authors thank the captain, crew, and technicians of the YK 14-19 cruise survey. Katsuhiko Suzuki, Tatsuo Nozaki, Saneatsu Saito, Yusuke Kubo, and Ken Takai, JAMSTEC researchers, greatly helped for data and discussion of the drillings in the Iheya North Knoll. This work was supported by the Cross-ministerial Strategic Innovation Promotion Program (SIP) "Next Generation Technology for Ocean Resources Exploration" and the Japan Society for the Promotion of Science KAKENHI (Grants 26289347, 18H03894, 18H03733, and 17J08764). We thank Marion Jegen, an anonymous reviewer, and Associate Editor Jeroen Ritsema for their very instructive comments. Some figures were produced with the aid of Generic Mapping Tools (GMT) software (https://www.soest.hawaii.edu/gmt). Data can be requested for scientific use through the website "JAMSTEC Data Site for Research Cruises" with cruise ID YK 14-19, accessed on 31 March 2019.

References

Allen, D., & Merrick, N. (2007). Robust 1D inversion of large towed geo-electric array datasets used for hydrogeological studies. *Exploration Geophysics*, *38*, 50–59. https://doi.org/10.1071/eg07003

Archie, G. E. (1942). The electrical resistivity log as an aid in determining some reservoir characteristics. *Transactions of AIME*, *146*(01), 54–62. https://doi.org/10.2118/942054-g

Bartetzko, A., Klitzsch, N., Iturrino, G., Kaufhold, S., & Arnold, J. (2006). Electrical properties of hydrothermally altered dacite from the PACMANUS hydrothermal field (ODP Leg 193). *Journal of Volcanology and Geothermal Research*, *152*, 109–120. https://doi.org/10.1016/j.jvolgeores.2005.10.002

Boschen, R. E., Rowden, A. A., Clark, M. R., & Gardner, J. P. A. (2013). Mining of deep-sea seafloor massive sulfides: A review of the deposits, their benthic communities, impacts from mining, regulatory frameworks and management strategies. *Ocean and Coastal Management*, *84*, 54–67. https://doi.org/10.1016/j.ocecoaman.2013.07.005

Cairns, G. W., Evans, R. L., & Edwards, R. N. (1996). A time domain electromagnetic survey of the TAG hydrothermal mound. *Geophysical Research Letters*, *23*(23), 3455–3458. https://doi.org/10.1029/96gl03233

Chave, A. D., Constable, S. C., & Edwards, R. N. (1991). *Electrical exploration methods for the seafloor. Electromagnetic Methods in Applied Geophysics*, (Vol. 2, pp. 931–966). Tulsa: Society of Exploration Geophysicists. https://doi.org/10.1190/1.9781560802686.ch12

Chiang, C. W., Goto, T., Mikada, H., Chen, C. C., & Hsu, S. K. (2012). Sensitivity of deep-towed marine electrical resistivity imaging using two-dimensional inversion: A case study on methane hydrate. *Terrestrial, Atmospheric and Oceanic Sciences*, *23*(6), 725–732. https://doi.org/10.3319/tao.2012.06.19.01(t)

Coggon, J. H. (1971). Electromagnetic and electrical modeling by the finite element method. *Geophysics*, *36*(1), 132–155. https://doi.org/10.1190/1.1440151

Constable, S., Kannberg, P. K., & Weitemeyer, K. (2016). Vulcan: A deep-towed CSEM receiver. *Geochemistry, Geophysics, Geosystems*, *17*, 1042–1064. https://doi.org/10.1002/2015gc006174

Constable, S., Kowalczyk, P., & Bloomer, S. (2018). Measuring marine self-potential using an autonomous underwater vehicle. *Geophysical Journal International*, *215*(1), 49–60. https://doi.org/10.1093/gji/ggy263

Constable, S., Parker, R., & Constable, C. (1987). Occam's inversion: A practical algorithm for generating smooth models from electromagnetic sounding data. *Geophysics*, *52*(3), 289–300. https://doi.org/10.1190/1.1442303

Dakhnov, V. N. (1962). Geophysical well logging. *Q. Colorado Sch. Mines*, *57*-2, 445 pp. Retrieved from https://www.tib.eu/en/search/id/TIBKAT%3A471153370/Geophysical-well-logging-the-application-of-geophysical/

Dey, A., & Morrison, H. F. (1979). Resistivity modelling for arbitrarily shaped two-dimensional structures. *Geophysical Prospecting*, *27*(1), 106–136. https://doi.org/10.1111/j.1365-2478.1979.tb00961.x

Expedition 331 Scientists (2010). Deep hot biosphere. IODP Prel. Rept., 331. https://doi.org/10.2204/iodp.pr.331.2010

Gehrmann, R., North, L. J., Graber, S., Szitkar, F., Petersen, S., Minshull, T. A., & Murton, B. J. (2019). Marine mineral exploration with controlled source electromagnetics at the TAG hydrothermal field, 26°N Mid-Atlantic Ridge. *Geophysical Research Letters*, *46*, 5808–5816. https://doi.org/10.1029/2019gl082928

Goto, T. N., Imamura, N., Mikada, H., Takekawa, J., Kasaya, T., & Sayanagi, K. (2013). Electromagnetic survey around the seafloor massive sulfide using autonomous underwater vehicle. In *Proceedings of the 11th SEGJ International Symposium* (pp. 342–345). Yokohama: Society of Exploration Geophysicists of Japan. https://doi.org/10.1190/segj112013-087

Goto, T. N., Kasaya, T., Machiyama, H., Takagi, R., Matsumoto, R., Okuda, Y., et al. (2008). A marine deep-towed DC resistivity survey in a methane hydrate area, Japan Sea. *Exploration Geophysics*, *39*(1), 52–59. https://doi.org/10.1071/eg08003

Hannington, M. D., Jonasson, I. R., Herzig, P. M., & Petersen, S. (1995). Physical and chemical processes of seafloor mineralization at mid-ocean ridges. *Seafloor Hydrothermal Systems: Physical, Chemical, Biological, and Geological Interactions*, *91*, 115–157. https://doi.org/10.1029/gm091p0115

Haroon, A., Hölz, S., Gehrmann, R. A., Attias, E., Jegen, M., Minshull, T. A., & Murton, B. J. (2018). Marine dipole–dipole controlled source electromagnetic and coincident-loop transient electromagnetic experiments to detect seafloor massive sulphides: Effects of three-dimensional bathymetry. *Geophysical Journal International*, *215*(3), 2156–2171. https://doi.org/10.1093/gji/ggy398

Humphris, S. E., Herzig, P. M., Miller, D. J., Alt, J. C., Becker, K., Brown, D., et al. (1995). The internal structure of an active sea-floor massive sulphide deposit. *Nature*, *377*(6551), 713. https://doi.org/10.1038/377713a0

Imamura, N., Goto, T. N., Kasaya, T., & Machiyama, H. (2018). Robust data processing of noisy marine controlled-source electromagnetic data using independent component analysis. *Exploration Geophysics*, *49*(1), 21–29. https://doi.org/10.1071/eg17139

Inoue, M. (2005). Development and case studies of the new submarine electric sounding system. *Geophysical Exploration*, *58*, 241–250 (in Japanese). https://doi.org/10.3124/segj.58.241

Ishizu, K., Vachiratienchai, C., Siripunvaraporn, W., Goto, T., Kasaya, T., & Iwamoto, H. (2017). Two-dimensional inversion of marine DC resistivity using fuzzy C-means clustering constraint. *87th Annual International Meeting, SEG, Expanded Abstracts*, 1204–1208. https://doi.org/10.1190/segam2017-17729696.1

Ishizu, K., Vachiratienchai, C., Siripunvaraporn, W., Goto, T., Kasaya, T., & Iwamoto, H. (2019). Evaluations of effectiveness of marine deep-towed DC resistivity survey in investigation of seafloor massive sulfide deposits. *Geophysical Exploration*, *72*, 122–138 (in Japanese). https://doi.org/10.3124/segj.72.122

Kasaya, T., Goto, T., Iwamoto, H., & Kawada, Y. (2018). Development of multi-purpose electromagnetic survey instruments. In *Proceedings of the 13th SEGJ International Symposium* (pp. 159–161). Tokyo: Society of Exploration Geophysicists of Japan. https://doi.org/10.1190/SEGJ2018-042.1

Kasaya, T., Machiyama, H., Kitada, K., & Nakamura, K. (2015). Trial exploration for hydrothermal activity using acoustic measurements at the North Iheya Knoll. *Geochemical Journal*, *49*(6), 597–602. https://doi.org/10.2343/geochemj.2.0389

Kawagucci, S., Chiba, H., Ishibashi, J. I., Yamanaka, T., Toki, T., Muramatsu, Y., et al. (2011). Hydrothermal fluid geochemistry at the Iheya North field in the mid-Okinawa Trough: Implication for origin of methane in subseafloor fluid circulation systems. *Geochemical Journal*, *45*(2), 109–124. https://doi.org/10.2343/geochemj.1.0105

Kawagucci, S., Miyazaki, J., Nakajima, R., Nozaki, T., Takaya, Y., Kato, Y., et al. (2013). Post-drilling changes in fluid discharge pattern, mineral deposition, and fluid chemistry in the Iheya North hydrothermal field, Okinawa Trough. *Geochemistry, Geophysics, Geosystems*, *14*, 4774–4790. https://doi.org/10.1002/2013gc004895

Keller, G. V. (1988). Rock and mineral properties. In *Electromagnetic Methods in Applied Geophysics* (Vol. 1, pp. 13–52). Tulsa: Society of Exploration Geophysicists. https://doi.org/10.1190/1.9781560802631.ch2

Key, K. (2009). 1D inversion of multicomponent, multifrequency marine CSEM data: Methodology and synthetic studies for resolving thin resistive layers. *Geophysics*, *74*(2), F9–F20. https://doi.org/10.1190/1.3058434

Key, K., & Weiss, C. (2006). Adaptive finite-element modeling using unstructured grids: The 2D magnetotelluric example. *Geophysics*, *71*(6), G291–G299. https://doi.org/10.1190/1.2348091

Komori, S., Masaki, Y., Tanikawa, W., Torimoto, J., Ohta, Y., Makio, M., et al. (2017). Depth profiles of resistivity and spectral IP for active modern submarine hydrothermal deposits: A case study from the Iheya North Knoll and the Iheya Minor Ridge in Okinawa Trough, Japan. *Earth, Planets and Space*, *69*(1), 114. https://doi.org/10.1186/s40623-017-0691-6

Kowalczyk, P. (2008). Geophysical prelude to first exploitation of submarine massive sulphides. *First Break*, *26*(11). Retrieved from). http://www.earthdoc.org/publication/publicationdetails/?publication=28613

Kumagai, H., Tsukioka, S., Yamamoto, H., Tsuji, T., Shitashima, K., Asada, M., et al. (2010). Hydrothermal plumes imaged by high-resolution side-scan sonar on a cruising AUV, Urashima. *Geochemistry, Geophysics, Geosystems*, *11*(12), Q12013. https://doi.org/10.1029/2010gc003337

Kwon, H. S., Kim, J. H., Ahn, H. Y., Yoon, J. S., Kim, K. S., Jung, C. K., et al. (2005). Delineation of a fault zone beneath a riverbed by an electrical resistivity survey using a floating streamer cable. *Exploration Geophysics*, *36*(1), 50–58. https://doi.org/10.3124/segj.58.50

Letouzey, J., & Kimura, M. (1986). The Okinawa Trough: Genesis of a back-arc basin developing along a continental margin. *Tectonophysics*, *125*, 209–230. https://doi.org/10.1016/0040-1951(86)90015-6

Lile, O. B., Backe, K. R., Elvebakk, H., & Buan, J. E. (1994). Resistivity measurements of the sea bottom to map fracture zones in the bedrock underneath sediments. *Geophysical Prospecting*, *42*, 813–824. https://doi.org/10.1111/j.1365-2478.1994.tb00242.x

Lipton, I. (2012). Mineral Resource Estimate Solwara Project Bismarck Sea PNG. *Technical Report under NI43-101*, 217 pp. Retrieved from http://www.nautilusminerals.com/irm/content/pdf/SL01-NSG-DEV-RPT-7020-001_Rev_1_Golder_Resource_Report.pdf

Masaki, Y., Kinoshita, M., Inagaki, F., Nakagawa, S., & Takai, K. (2011). Possible kilometer-scale hydrothermal circulation within the Iheya-North field, mid-Okinawa Trough, as inferred from heat flow data. *JAMSTEC Report of Research and Development*, *12*, 1–12. https://doi.org/10.5918/jamstecr.12.1

Miyoshi, Y., Ishibashi, J. I., Shimada, K., Inoue, H., Uehara, S., & Tsukimura, K. (2015). Clay minerals in an active hydrothermal field at Iheya-North-Knoll, Okinawa Trough. *Resource Geology*, *65*(4), 346–360. https://doi.org/10.1111/rge.12078

Momma, H., Iwase, R., Mitsuzawa, K., Kaiho, Y., Fujiwara, Y., Amitani, Y., & Aoki, M. (1996). Deep tow survey in Nanseisyoto region (K95-07-NSS), *JAMSTEC. Journal of Deep-Sea Research*, *12*, 195–210 (in Japanese with English abstract). Retrieved from http://www.godac.jamstec.go.jp/catalog/data/doc_catalog/media/shinkai12_16.pdf

Müller, H., Schwalenberg, K., Reeck, K., Barckhausen, U., Schwarz-Schampera, U., Hilgenfeldt, C., & von Dobeneck, T. (2018). Mapping seafloor massive sulfides with the Golden Eye frequency-domain EM profiler. *First Break*, *36*(11), 61–67. Retrieved from. http://www.earthdoc.org/publication/publicationdetails/?publication=94767

Nakagawa, S., Takai, K., Inagaki, F., Chiba, H., Ishibashi, J., Kataoka, S., et al. (2005). Variability in microbial community and venting chemistry in a sediment-hosted backarc hydrothermal system: Impacts of subseafloor phase-separation. *FEMS Microbiology Ecology*, *54*, 141–155. https://doi.org/10.1016/j.fems.2005.03.007

New Energy and Industrial Technology Development Organization (1995). Report of exploration for development of geothermal power in west Aso area, 1507 pp (in Japanese). Retrieved from http://geothermal.jogmec.go.jp/gathering/file/57.pdf

Ohta, Y., Goto, T., Koike, K., Kashiwaya, K., Lin, W., Tadai, O., et al. (2018). Construction of rock physics model based on electrical conductivity characteristics of rock samples obtained in seafloor hydrothermal areas. *Geophysical Exploration*, *71*(in Japanese), 43–55. https://doi.org/10.3124/segj.71.43

Petersen, S., Herzig, P. M., & Hannington, M. D. (2000). Third dimension of a presently forming VMS deposit: TAG hydrothermal mound, Mid-Atlantic Ridge, 26 N. *Mineralium Deposita*, *35*(2–3), 233–259. https://doi.org/10.1007/s001260050018

Petersen, S., Monecke, T., Westhues, A., Hannington, M. D., Gemmell, J. B., Sharpe, R., et al. (2014). Drilling shallow-water massive sulfides at the Palinuro volcanic complex, Aeolian island arc, Italy. *Economic Geology*, *109*(8), 2129–2158. https://doi.org/10.2113/econgeo.109.8.2129

Quist, A. S., & Marshall, W. L. (1968). Electrical conductances of aqueous sodium chloride solutions from 0 to 800 degrees and at pressures to 4000 bars. *The Journal of Physical Chemistry*, *72*(2), 684–703. https://doi.org/10.1021/j100848a050

Revil, A., Aal, G. Z. A., Atekwana, E. A., Mao, D., & Florsch, N. (2015a). Induced polarization response of porous media with metallic particles—Part 2: Comparison with a broad database of experimental data. *Geophysics*, *80*, D539–D552. https://doi.org/10.1190/geo2014-0578.1

Revil, A., Florsch, N., & Mao, D. (2015b). Induced polarization response of porous media with metallic particles—Part 1: A theory for disseminated semiconductors. *Geophysics*, *80*, D525–D538. https://doi.org/10.1190/geo2014-0577.1

Rona, P. A., Palmer, D. R., Jones, C., Chayes, D. A., Czarnecki, M., Carey, E. W., & Guerrero, J. C. (1991). Acoustic imaging of hydrothermal plumes, East Pacific Rise, 21°N, 109°W. *Geophysical Research Letters*, *18*, 2233–2236. https://doi.org/10.1029/91gl02897

Safipour, R., Hölz, S., Jegen, M., & Swidinsky, A. (2017). On electric fields produced by inductive sources on the seafloor. *Geophysics*, *82*(6), E297–E313. https://doi.org/10.1190/geo2016-0700.1

Safipour, R., Hölz, S., Jegen, M., & Swidinsky, A. (2018). A first application of a marine inductive source electromagnetic configuration with remote electric dipole receivers: Palinuro Seamount, Tyrrhenian Sea. *Geophysical Prospecting*, *66*(7), 1415–1432. https://doi.org/10.1111/1365-2478.12646

Saito, S., Sanada, Y., Moe, K., Kido, Y. N., Hamada, Y., Kumagai, H., et al. (2015). Identification and characterization of the active hydrothermal deposits in Okinawa Trough, SW Japan: Estimates from logging-while-drilling. *AGU Fall Meeting Abstracts*. San Francisco. Retrieved from https://agu.confex.com/agu/fm15/webprogram/Paper77585.html

Schwalenberg, K., Rath, V., & Haak, V. (2002). Sensitivity studies applied to a two-dimensional resistivity model from the Central Andes. *Geophysical Journal International*, *150*(3), 673–686. https://doi.org/10.1046/j.1365-246x.2002.01734.x

Shewchuk, J. R. (1996). Triangle: Engineering a 2D quality mesh generator and Delaunay triangulator. In *Applied Computational Geometry towards Geometric Engineering*, (pp. 203–222). Berlin, Heidelberg: Springer. https://doi.org/10.1007/bfb0014497

Siripunvaraporn, W., & Egbert, G. (2000). An efficient data-subspace inversion method for 2-D magnetotelluric data. *Geophysics*, *65*(3), 791–803. https://doi.org/10.1190/1.1444778

Spagnoli, G., Hannington, M., Bairlein, K., Hördt, A., Jegen, M., Petersen, S., & Laurila, T. (2016). Electrical properties of seafloor massive sulfides. *Geo-Marine Letters*, *36*, 235–245. https://doi.org/10.1007/s00367-016-0439-5

Stein, C., & Stein, S. (1992). A model for the global variation in oceanic depth and heat flow with lithospheric age. *Nature*, *359*, 123–129. https://doi.org/10.1038/359123a0

Takai, K., Kumagai, H., Kubo, Y., & CK1404 on-board member (2015). Cruise report SIP-HOT I "Pathfinder" (SIP-Hydrothermal deposit in Okinawa Trough) CK14-04 (Exp. 907), JAMSTEC, Yokosuka, 116 pp. Retrieved from http://www.godac.jamstec.go.jp/catalog/data/doc_catalog/media/CK14-04-907_all.pdf (accessed on March 31, 2019)

Takai, K., Mottl, M. J., Nielsen, S. H., & The Expedition 331 Scientists (2011). *Proceedings of the Integrated Ocean Drilling Program*, (Vol. 331). Washington, DC: Integrated Ocean Drilling Program Management International, Inc. https://doi.org/10.2204/iodp.proc.331.2011

Takai, K., Nakagawa, S., Reysenbach, A. L., & Hoek, J. (2006). Microbial ecology of mid-ocean ridges and back-arc basins. *Geophysical Monograph—American Geophysical Union*, *166*, 185–213. https://doi.org/10.1029/166gm10

Tornos, F., Peter, J. M., Allen, R., & Conde, C. (2015). Controls on the siting and style of volcanogenic massive sulphide deposits. *Ore Geology Reviews*, *68*, 142–163. https://doi.org/10.1016/j.oregeorev.2015.01.003

Tsuji, T., Takai, K., Oiwane, H., Nakamura, Y., Masaki, Y., Kumagai, H., et al. (2012). Hydrothermal fluid flow system around the Iheya North Knoll in the mid-Okinawa trough based on seismic reflection data. *Journal of Volcanology and Geothermal Research*, *213*, 41–50. https://doi.org/10.1016/j.jvolgeores.2011.11.007

Vachiratienchai, C., & Siripunvaraporn, W. (2013). An efficient inversion for two-dimensional direct current resistivity surveys based on the hybrid finite difference–finite element method. *Physics of the Earth and Planetary Interiors*, *215*, 1–11. https://doi.org/10.1016/j.pepi.2012.10.012

Von Herzen, R. P., Kirklin, J., & Becker, K. (1996). Geoelectrical measurements at the TAG hydrothermal mound. *Geophysical Research Letters*, *23*(23), 3451–3454. https://doi.org/10.1029/96gl02077

Xu, S. Z., Duan, B. C., & Zhang, D. H. (2000). Selection of the wavenumbers k using an optimization method for the inverse Fourier transform in 2.5D electrical modelling. *Geophysical Prospecting*, *48*(5), 789–796. https://doi.org/10.1046/j.1365-2478.2000.00210.x